# "Layered Materials as High Temperature Membranes in Hydrogen Production"

**FINAL TECHNICAL REPORT**

**Project Start Date: August 17, 2005 Project End Date: August 16, 2006**

**Principal Authors: Muhammad Sahimi and Theodore T. Tsotsis**

**Date of Report: November 26, 2006**

**DOE Award No. DE-FG26-05NT42541**

**University of Southern California**

**Mork Family Department of Chemical Engineering and Materials Science**

**925 Bloom Walk, HED-216**

**Los Angeles, CA 90089-1211**

## DISCLAIMER

## ABSTRACT

The objective of this project is the development of a new high temperature, affinity-type $CO_2$-selective membrane. This membrane has the potential to find use in novel reactive applications of relevance to IGCC plants. In this project we have utilized a variety of methods to prepare affinity-type $CO_2$-selective membranes. We have used a number of hydrotalcite (HT) sources and supports. We have also prepared two types of membranes, large area membrane disks and tubes, and micromembranes prepared on stainless steel foils and silicon wafers. Quality nanoporous membranes have been prepared, which show significantly higher permeation rates for gases with smaller kinetic diameters like He (used here as a safe surrogate gas for hydrogen) as compared to gases with larger kinetic diameters like Ar. Some of these membranes are selective towards $CO_2$. The effect of preparation conditions on the membrane transport characteristics have also been studied and are reported here.

## TABLE OF CONTENTS

# 1. Executive Summary

## 1.1 Objectives

IGCC plants show promise for environmentally-benign power generation. In these plants coal is gasified to synthesis gas, which is then processed in a water gas-shift reactor (WGSR) to produce $H_2$ for clean-power generation. WGSR is a dual-reactor system, the first reactor (HTS) operating at high temperatures, to attain high reaction rates, followed by a second lower-temperature reactor (LTS), which benefits from increased equilibrium conversions at low temperatures. The WGSR exit stream contains $H_2$, $CO_2$, $H_2O$ and other minor species (e.g., CO). For use in fuel cells (and potentially for $CO_2$ capture/sequestration), $CO_2$ is separated using amine absorption or PSA. Both processes are, however, energy- and capital-intensive, and so is the WGSR. In their place our team proposes, instead, a novel membrane reactor (WGSMR), which integrates the WGS and $CO_2$ separation steps in a single unit through the use of high temperature, $CO_2$-selective membranes. The WGSMR has many advantages over the conventional technology. Key to the success of the WGSMR is developing $CO_2$-selective membranes, capable of operating in the WGS environment, since commercial membranes are not functional in this environment. The objective of this project is, therefore, the development of a new high temperature, affinity-type $CO_2$-selective membrane.

## 1.2 Accomplishments to Date

We have utilized a variety of methods to prepare affinity-type $CO_2$-selective membranes. We have used a number of hydrotalcite (HT) sources and supports. We have also prepared two types of membranes, large area membrane disks and tubes, and micromembranes prepared on stainless steel foils and silicon wafers. The micromembranes show good potential for application in micro-fuel cells. The membranes have been tested for their transport characteristics using both single gases and mixtures of gases, as well as by a variety of other characterization techniques including SEM and TEM, DRIFTS, EDX, and DTA/TGA. Quality nanoporous membranes have been prepared, which show significantly higher permeation rates for gases with smaller kinetic diameters like He (used here as a safe surrogate gas for hydrogen) as compared to gases with larger kinetic diameters like Ar. Some of these membranes are selective towards $CO_2$. The effect of preparation conditions on the membrane transport characteristics have also been studied and are reported here. Coating the membranes with a silicone layer, which helps to plug the pore space within the HT structure, creates a membrane which is highly selective towards $CO_2$.

## 2. Results of Work

### 2.1.Project Approach

The objective of the project was to utilize variety of methods to prepare affinity-type $CO_2$-selective membranes. The plan was to utilize a number of hydrotalcite (HT) sources and membrane supports, and to test the membranes for their transport characteristics using both single gases and mixtures of gases, as well as by a variety of other characterization techniques, including SEM and TEM, DRIFTS, EDX, and DTA/TGA. The plan was also to prepare two different types of membranes, namely large-area membrane disks and tubes, and micromembranes prepared on stainless steel foils and silicon wafers. The micromembranes show good potential for application in micro-fuel cells.

### 2.1.1 Large Area Membrane Preparation

To prepare the HT membranes, we have utilized a variety of HT sources including commercial hydrotalcite powders from Sasol and Aldrich; we have also synthesized a number of such materials ourselves by the co-precipitation method[1], as follows: An aqueous solution (45 ml) containing 0.058 mol of $Mg(NO_3)_2{\cdot}6H2O$ and 0.02 mol of $Al(NO_3)_3{\cdot}9H_2O$ (ACS reagent grade, purchased from Aldrich) is prepared (Mg/Al molar ratio of 2.9:1).. This solution is added all at once to a second solution (70 ml) containing NaOH (0.35 mol) and $Na_2CO_3$ (0.09 mol) at 333K. The resulting mixture is kept at this temperature for 24 h under vigorous stirring, after which the white precipitate that was formed was filtered off and washed with distilled water several times. The hydrotalcite was dried for 24 h at 393 K. Using ICP-MS analysis, the synthetic hydrotalcite was shown to have a Mg/Al ratio of 2.89:1 (this HT is labeled as HT1; another HT with a different Mg/Al ratio was also prepared, labeled as HT2). The commercial hydrotalcites were also analyzed by ICP-MS. Table 1 shows the various HT we utilized with their corresponding Mg/Al molar ratios.

The powders, thus prepared, were also used to prepare macroporous HT disks as supports in membrane preparation. These membrane supports were prepared by pressing 3 g of HT with 1000 $kg_f/cm^2$ of pressure for 10 min. We have also utilized α- alumina tubes

(I.D 7 mm, O.D. 11mm, 0.5~1.0 μm pore radius, ~40% porosity) from the Dalian Institute in China, α-alumina discs prepared in our laboratories (using alumina powders from the Coors-Tek company), as well as γ-alumina tubes prepared by us by sol-gel techniques. In order to prepare microporous HT membranes, various methods were utilized including dip-coating, and electrophoretic deposition, as described below:

*Dip-coating*. For dip-coating, HT slurries were prepared by two different methods. The first method involved the HT2 solution (Table 1). After 2 h of reaction under vigorous stirring at a temperature of 60 $^{o}$C, distilled water was added to the reaction mixture, which was then centrifuged for 10 min at 2500 rpm in a sealed container. At the end of centrifugation, the supernatant solution was removed (this is defined as the mother solution); distilled water was again added to the thick slurry at the bottom of the container, which was then centrifuged again, the supernatant solution removed, etc. The procedure is repeated until the pH of the slurry becomes ~ 8.[2] The supernatant solution was then again removed, distilled water was added to the remaining residue and shaken vigorously. The resulting suspension was then allowed to stand for one day. The resulting mixture was separated in three layers, i.e. a dark bottom layer, a translucent middle layer, and a transparent top layer. The translucent layer was then recovered and utilized to prepare the HT membrane on α-alumina and γ-alumina supports. The mother solution was also used in the hydrothermal treatment at 80 $^{o}$C, 100 $^{o}$C, and 120 $^{o}$C. Another method involved dispersing the Sasol Mg70D powder in distilled water (this material is easily dispersible because it contains lactate acid, which acts as a dispersion agent). After the suspension was prepared, membrane support tubes were dipped in the suspension for 10 s at a time for each coating. The membranes were then dried overnight in air, and then at 150 $^{o}$C for 12 h.

*Using Sulfate as a Binder.* Some of the HT membranes were prepared using sulfate as a binder. 99% sulfuric acid (ACS reagent grade from VWR) was used as the sulfate source.[3] The Sasol Mg70D and Mg50 powders were utilized for the preparation. A 2 M $H_2SO_4$ solution was added drop-wise to the HT suspension (prepared by ultrasonic treatment for 15 min to assure that the HT disperses well). 1 g of Mg70D or 1 g of Mg50 were dispersed

**Table 1**. The Mg/Al ratio of HT powders

| HT material | Mg/Al ratio from ICP-MS | Synthesis Condition | |
|---|---|---|---|
| | | Mg/Al Molar Ratio | Reaction Conditions. |
| Sasol Mg50 | 1.29 | | |
| Sasol Mg70 | 3.0 | | |
| Sasol Mg70D[a] | 3.0 | - | - |
| Sasol Mg70DS[b] | 3.0 | - | - |
| Aldrich HT | 2.19 | - | - |
| Synthetic HT 1 | 2.89 | Mg/Al=2.9 | 24 h, 333K |
| Synthetic HT 2 | 3.1 | Mg/Al=3.0 | 2 h, 333K |

[a]: 4.6% lactate acid added to make the Mg70D HT disperse well

[b]: Resulting by particle reduction treatment by mall-billing from the Mg70D

in 2 ml or 9.5 ml of the 2 M $H_2SO_4$ solution respectively. The slurry was stirred for 24 h at 80 $^oC$. The membranes were prepared using α-alumina tubes as substrates, by dip-coating or by *in-situ* coating (during dip-coating the alumina tube stays in the solution for a few sec; *in-situ* coating requires more time in solution, typically ranging from 30 min to 3 h). After preparation, the Mg50-coated membrane was dried for 3 days in ambient air. The Mg70D-coated membrane was dried overnight in ambient air, and then at 150 $^oC$ for 24 h.

*Vacuum-Suction Method*. The vacuum-suction method was also used for the preparation of some of the membranes. [4] In membrane preparation we utilized the commercial

hydrotalcite (Mg70D), provided by Sasol. The Mg 70D powder size was reduced by ball-milling at the NETZSCH Corporation, its average particle size reduced from 12.8 to 0.17 μm (see Fig. 1). This HT powder is, hereinafter, referred to as Mg70DS (see Table 1).

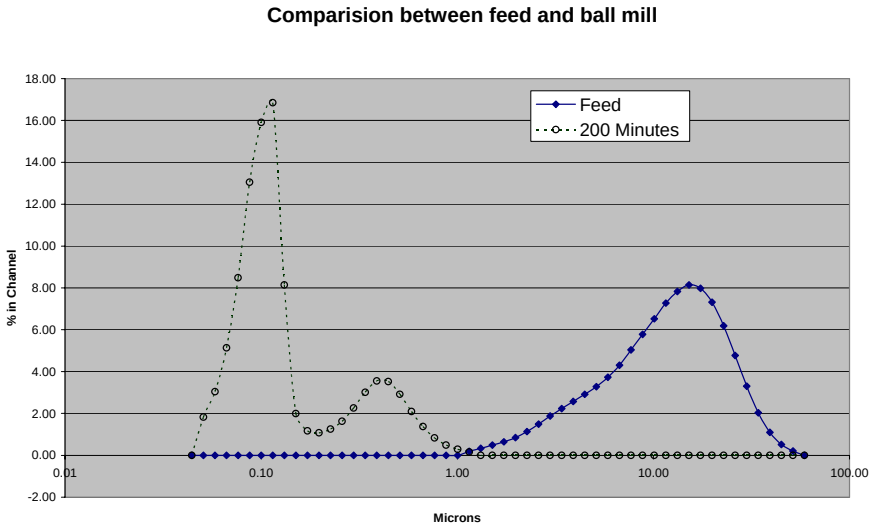


**Figure 1**. The particle size of Mg70D before and after ball-milling

Porous α-$Al_2O_3$ discs were used as supports for these membranes. The disks (2 mm thick), were prepared by pressing 7 g of alumina powder (purchased by Accumet Materials) with 1000 $kg_f/cm^2$ of pressure for 10 min. The disc was then calcined at 1000 $^oC$ for 3 h. The porosity of the supports was ~0.34 (as measured by the Archimedes method).The surface of the support was polished with 600 and 2400 grit-sand paper, and was then cleaned several times with deionized water in an ultrasonic bath. Before coating, the support was dried in air at 473K for 6 h. The colloidal HT suspension used for coating was prepared by dispersing the Mg70DS HT in deionized water (at a concentration of 0.76 wt%) with the aid of ultrasonic treatment. 2 ml of this solution was added drop-wise on the support, and a HT layer was formed on the top support surface using vacuum suction with the aid of a mechanical pump, which created vacuum from the bottom of support. The membranes, thus prepared, were dried at 150 $^oC$ for 12 h. Some membranes were, in addition, coated using a 3.5 wt.% silicone solution (GE Silicones, RTV 615A,B) in heptane

(from Aldrich), in order to improve their performance, also by using the vacuum-suction method. This treatment plugs the inter-crystallite space, and potentially the pinholes and cracks.

*Electrophoretic Deposition*. A number of membranes were also prepared by electrophoretic deposition (EPD), which involves the migration and coagulation of ceramic particles on an electrode surface aided by an electric field.[5,6] The advantages of EPD are the uniformity of the deposition process, even for complex and large forms, and good control of the thickness of the deposit. [7]During EPD, the mass of deposit is described by the following equation:

$$M = \int_{o}^{t} aAc\mu E dt \qquad (1)$$

where M is the of the mass of the deposit (kg), t the deposition time (s), α a coefficient related to the friction characteristics of the particles near the electrode that are being deposited, A the electrode surface area ($m^2$), C the particle concentration in the suspension ($kg/m^3$), μ the electrophoretic mobility ($m^2/Vs$**),** and E the electric field (V/m). The electrophoretic mobility ($m^2/Vs$) is given by the following equation

$$\mu = \frac{ZEV}{4\pi L\eta} \qquad (2)$$

where *Z* is the zeta potential, *V* the applied voltage, *E* the dielectric constant of the medium in which the particles are suspended, η the viscosity of the suspension, and L the electrode separation distance. As Equation (2) indicates, electromobility depends on the zeta potential.[8,9,10] The zeta potential, is an intrinsic property of each slurry system, and is the potential between the Stern layer and the Diffuse layer (as defined in the double-layer colloidal model); its value determines which electrode is the target for deposition during EPD. In our study, the zeta potential was measured by a Zeta Meter 3.0 (Zeta-Meter Inc.).

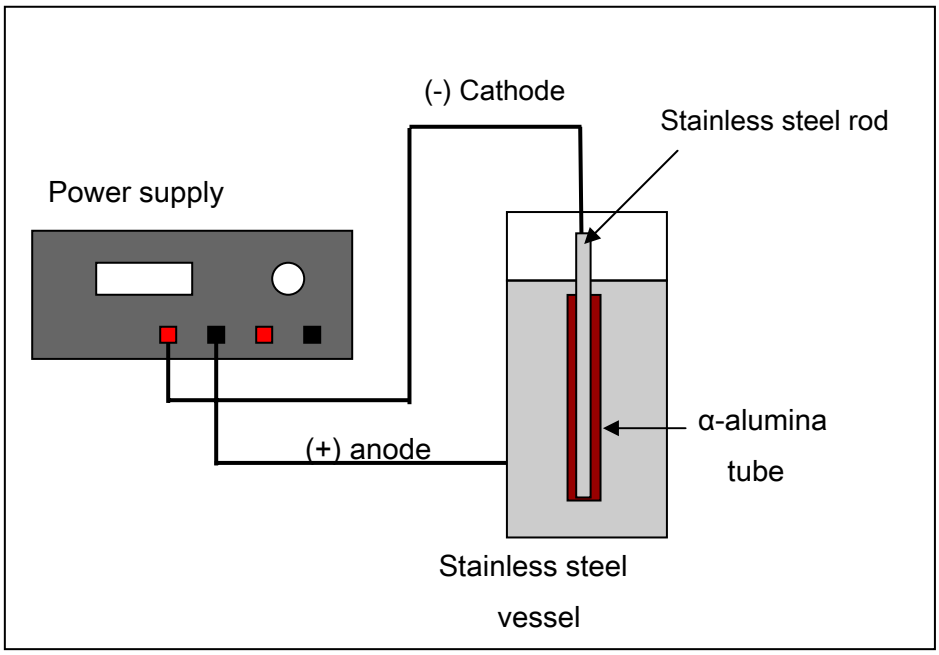


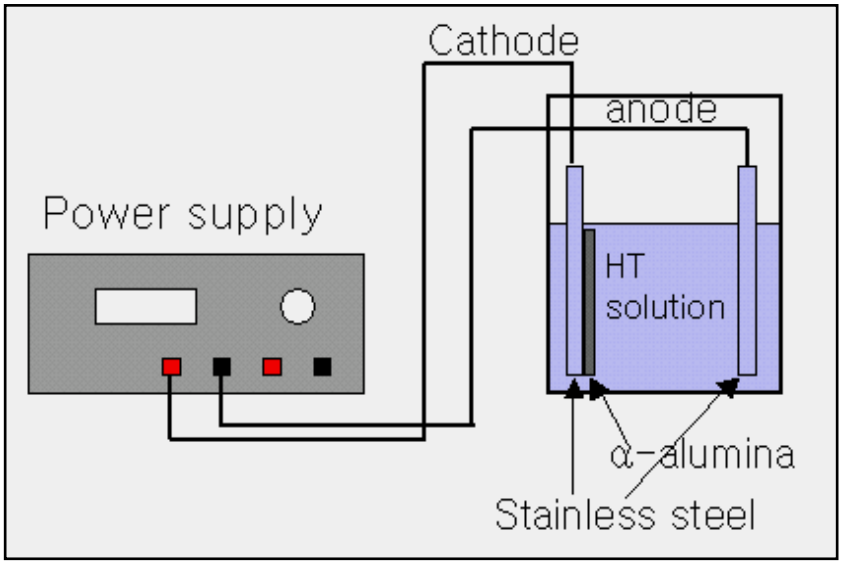


**Figure 2**. EPD membrane preparation apparatus.

For EPD, the Sasol Mg70DS powder was used to prepare a suspension in distilled water. Porous α- alumina tubes or discs were used as the supports. The EPD unit is illustrated

schematically in Fig. 2.[7,11] For deposition on the tubular membranes, a stainless steel rod was inserted inside the support tube to be used as the cathode. The stainless steel vessel itself was used as the anode (the choice in electrodes varies, depending on the zeta potential). A DC power supply was used to generate the potential difference between the two electrodes. The electrical potential varied from 1 to 20 V, while the HT weight fraction in the colloidal suspension varied between 0.38 ~ 1.25 wt %. The solution's pH was adjusted by using 0.9 M $H_2SO_4$ and 0.9 M NaOH solutions. The membranes, after coating, were dried overnight in ambient air, and at 150 °C for 12 h.

### 2.1.2 Micro-Membrane Preparation

In this study, we have also investigated the fabrication of HT micromembranes using silicon wafers and stainless steel foils as templates. Using (100) p-type silicon wafers we have created a microchannel pattern as shown in Fig. 3. It consists of two different channel types, with a width of 500 and 1000 μm correspondingly, which were fabricated using a standard photolithographic technique[12,13]

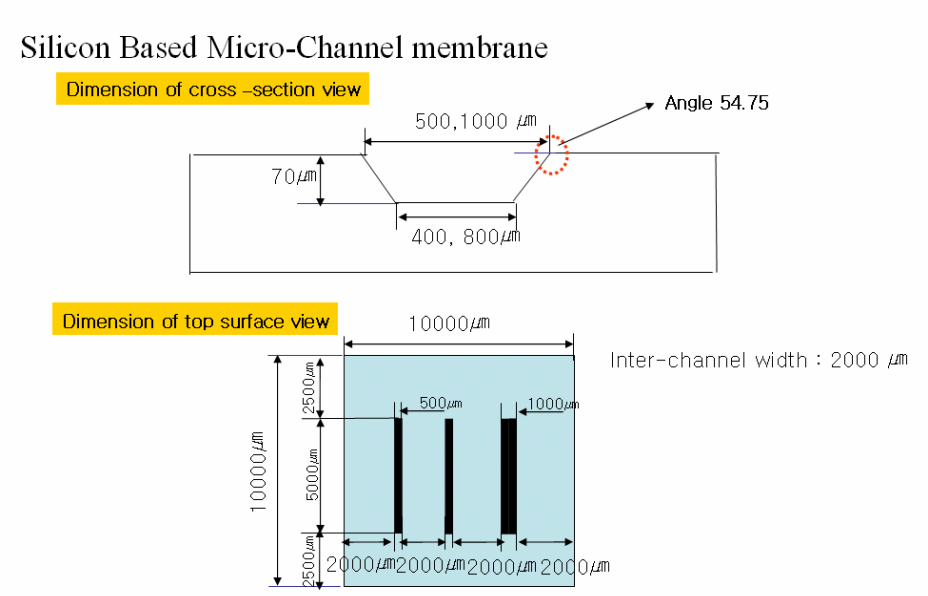


**Figure 3**. The silicon microchannels

The channels were etched using a 44 wt% KOH solution at 359 K. The anisotropic wet-etching rates along the silicon <111> and <100> directions result in a trapezoidal channel cross-section with an angle of 54.7°, as shown in Fig. 3. After the microchannel was prepared, it was coated with HT using various coating methods, with or without an intermediate support layer. (see Table 2). After the HT coating process finishes, self-standing HT micromembranes are prepared by wet-etching of the silicon layer at the bottom of the HT layer using a 44 wt% KOH solution at 359 K.

We have also prepared micromembranes on stainless steel supports. These membranes are, potentially, more useful than the Si-wafer-based membranes, due to their better mechanical properties. A simple design (see Fig. 4), consisting of a square pattern of small circular holes (microholes), each with a diameter of 800 μm, is typically fabricated by conventional drilling. The micromembrane is prepared by coating these microholes with a solution containing 20 wt% Mg70DS, and drying at 150 $^{o}$C for 24 h.

**Table 2**. Various coating methods used for the preparation of Si-based HT micromembranes

| No | Intermediate layer | Coating method | Conditions |
|---|---|---|---|
| 1 | None | Colloidal HT coating drop-wise by a micropipette | Dry at 110℃ for 12 h |
| 2 | | Seed deposition followed by hydrothermal aging | Dry at 110℃ for 12 h (after seed deposition)<br>160 $^{o}$C for 24 h (hydrothermal aging) |
| 3 | γ-alumina | Colloidal HT coating drop-wise by a micropipette | Dry at 110℃ for 12 h |

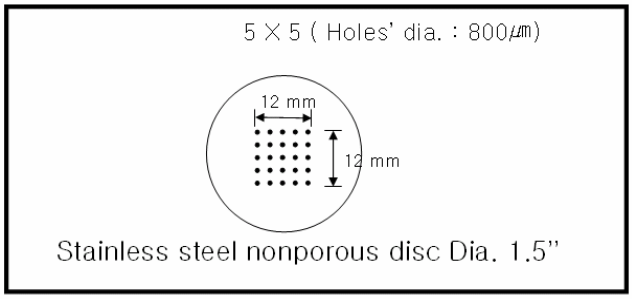


**Figure 4**. The microhole pattern on stainless steel disks

### 2.1.3 Membrane Characterization

FT-IR was used to characterize the various HT materials generated. The FT-IR spectra were recorded using a Genesis II (Mattson, FT-IR) instrument; the instrument operating conditions were a scan-range from 4000 $cm^{-1}$ to 500 $cm^{-1}$, scan numbers 16, and a scan resolution of 2 $cm^{-1}$. We also utilized XRD to characterize the HT materials, using a Rigaku X-ray diffractometer, with the $CuK_{\alpha}$ line for the X-ray source with a monochromator positioned in front of the detector. Scans were performed over a 2θ range from $5^{o}$ to $75^{o}$. Thermogravimetric (TG) curves were generated using a Cahn TGA 121 instrument. The sample (~100 mg) was heated in UHP dry argon (at a flow rate of 30 ml/min) with a heating rate of 5 $^{o}$C/min, till 700 $^{o}$C. A Micrometrics ASAP 2010 BET instrument was used for measuring the surface area by the BET method at liquid nitrogen temperature (77 K); the micropore size and pore size distribution (PSD) of HT samples was also determined by the same instrument using the Horvath-Kawazoe (H-K) equation. The isotherms were measured using samples that had been preheated in vacuum at various temperatures overnight. The morphology and thickness of the synthesized membrane were investigated by scanning electron microscopy (SEM). The SEM photographs and the EDX (Energy Dispersive X-ray spectrometer) analysis were obtained using a Cambridge 360 scanning electron microscope, and a Philips/FEI XL-30 Field Emission Scanning Electron Microscope.

The HT membranes were also characterized by permeation measurements. The permeation apparatus used in this study consists of a permeation cell, He, Ar, $N_2$, $H_2$, CO,

and $CO_2$ gas cylinders, pressure gauges, a gas chromatograph, a mass-spectrometer, a syringe-pump (for delivering water to create synthetic WGS feeds), and a temperature–controlled oven. The membrane areas were 6.51 and 0.865 $cm^2$ for the tubular and disc membranes correspondingly. Water vapor in the permeation and feed-side exit streams was collected with moisture traps. The membrane permeances were measured using a bubble-flow meter for single gases, and a gas chromatograph or mass spectrometer for mixtures of gases. For the silicone-coated HT membranes, the constant volume, diffusion time-lag method was used**.** To measure the gas permeance, the permeate side pressure was kept around $1\times10^{-2}$ Torr, while the feed-side was maintained at a predetermined fixed pressure. Gas permeance is calculated from the change in pressure on the permeate side.

## 2.2 Results and Discussion

### 2.2.1 Characterization Results

#### 2.2.1.1 HT Powders

The FTIR spectra of one of the HT synthesized in our labs (HT1) and of the Sasol Mg70D HT are shown in Fig. 5.

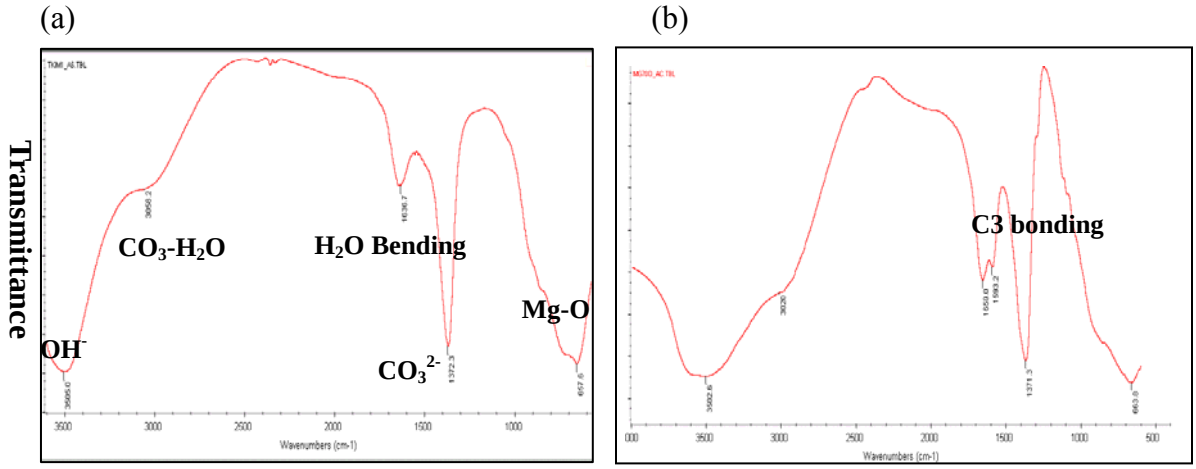


**Figure 5**. FT-IR spectra (a) of synthetic HT (b) Sasol Mg70D.

The spectra appear to be similar, with the exception of a band at 1593.2 $cm^{-1}$ in the Mg70D spectrum, which results from the lactate acid ($CH_3$-HCOH-COOH), which is added to the Sasol Mg70D powder to improve its dispersion characteristics. Typical XRD patterns for the synthetic and commercial HT are shown in Fig. 6.

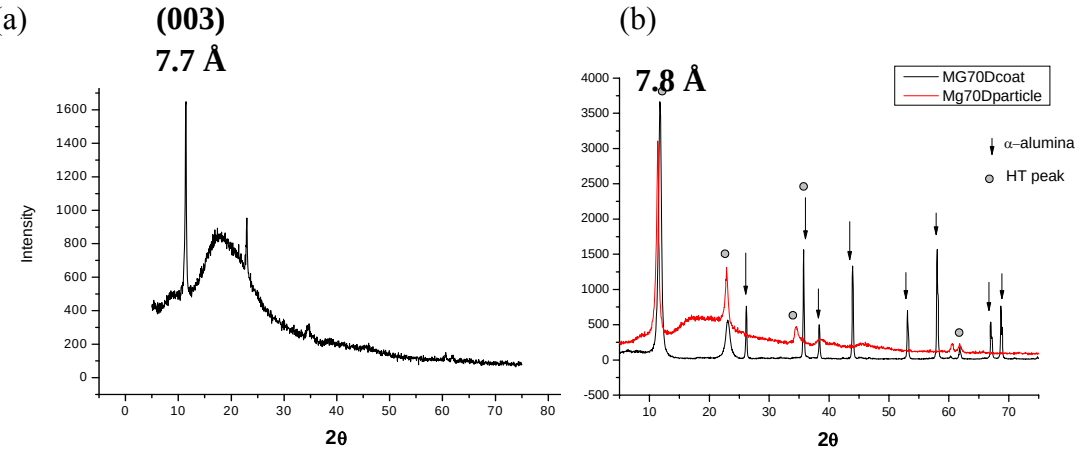


**Figure 6**. HT XRD patterns (a) own HT powder (b) Mg70D powder and membrane.

The basal spacing for the synthetic HT (calculated according to Bragg's equation) is 7.7 Å. The XRD patterns for the Sasol Mg70D HT indicate that the basal spacing is 7.8 Å. These results are similar to those reported in the literature, indicating a typical basal spacing of ~ 7.8 Å (for HT with a Mg/Al=3). [14]. The XRD spectrum of the surface of one of the HT membranes prepared by the vacuum-suction method is shown in Fig. 6b, and combines the spectral peaks for both alumina and the overlaying HT film.

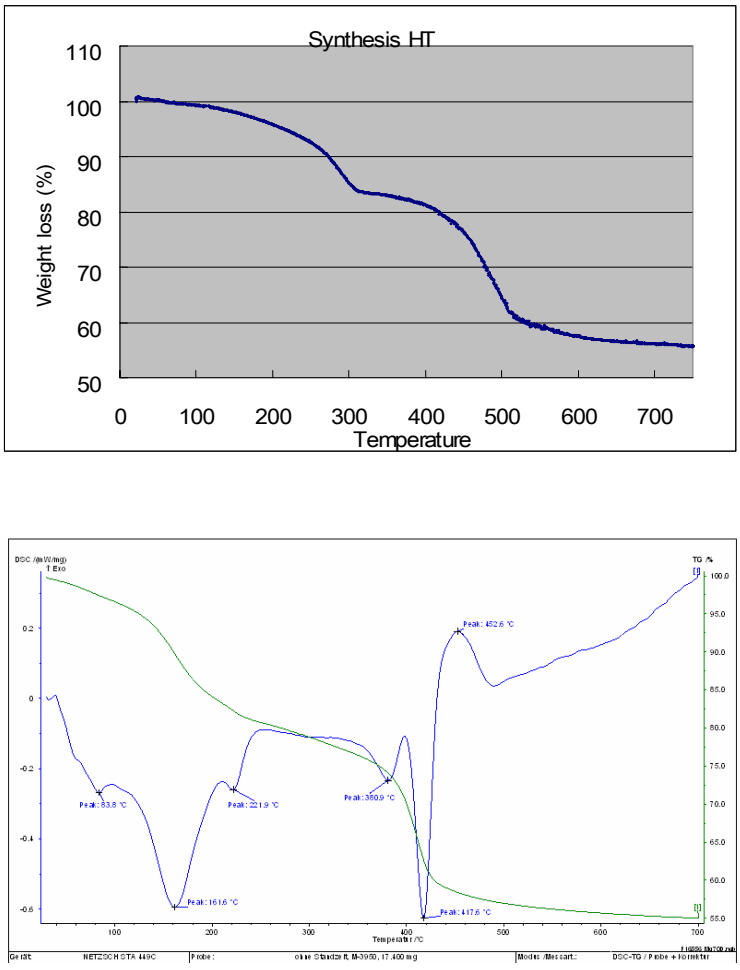


**Figure 7**. TGA thermograms of the synthetic HT (top) and the Sasol Mg70D (bottom)

Figure 7 shows the thermograms for both the synthetic (HT1) and the Sasol Mg70D HT. They appear to be typical HT thermograms. There are some differences between the two samples, however, which may be due to the different heat treatment conditions, and

the presence of the dispersion agent in the Sasol Mg 70D. Figure 7 (bottom) also shows the DSC spectrum of the Mg70D HT. Endothermic peaks are observed due to desorption of water, and lactate acid, and to the loss of $OH^-$ groups present in the interlayer region. $CO_3^{2-}$ anion elimination is an exothermic reaction manifested by an intense exothermic peak at 452.6 $^oC$.

The pore structure was evaluated by analysis of BET data. The microporosity was evaluated using the H-K equation with a slit-type pore model, while mesoporosity was evaluated using the BJH model. Analysis results are shown in Table 3.

**Table 3.** Surface area and pore size of HT powder

| | Pretreatment temp. ($^oC$) | Surface area ($m^2/g$) | BJH adsorption, average pore size | H-K median pore size |
|---|---|---|---|---|
| Sasol Mg70D (uncalcined) | 150 | 1.5 | 18.0 nm | 10.7 Å |
| | 300 | 23.8 | 12.3 nm | 8 Å |
| Sasol Mg70D (calcined@550 $^oC$) | 150 | 219.9 | 3.1 nm | 8.4 Å |
| Synthetic HT (uncalcined) | 120 | 26.1 | 33.9 nm | 9.2 Å |

The surface area of the samples is low, and increases with increasing calcination temperature. High temperature treatment decreases the pore size. The observed isotherms are of Type II

Figure 8 shows the top surface of a membrane (at two different magnifications) prepared by the vacuum-suction method. The membrane has a smooth top surface, probably due to the very small size of the Mg70DS powder used to prepare the membrane. Figure 9a shows the cross-section of one of these membranes. The film

thickness is around 6 ~ 7 µm, and the layer appears to consist of well-intergrown HT crystallites without defects. Figure 9b shows the cross-section of one of the silicone-coated HT membranes. One clearly sees in this Figure the HT layer and the silicone layer sitting on the top of the HT layer. The total film thickness is ~10 µm.

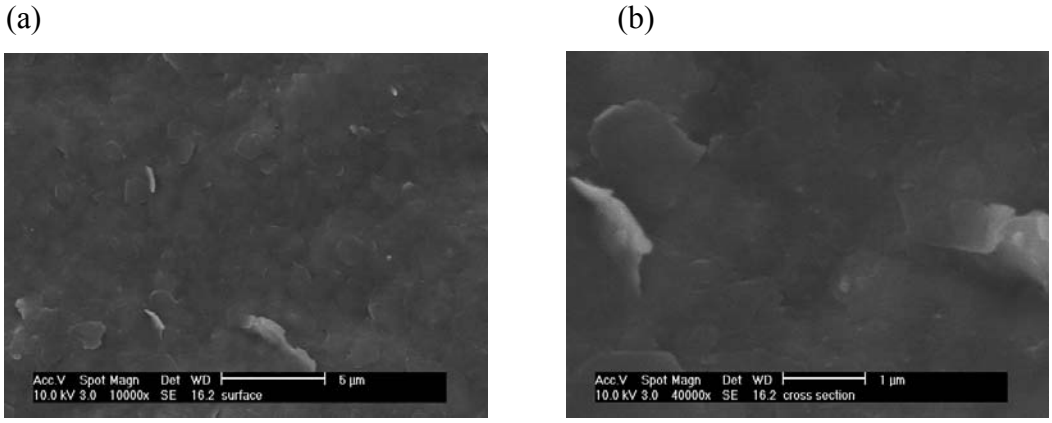


**Figure 8**. SEM picture of a vacuum-suction membrane (a) Magnification ×10K (b) Magnification ×40K (top view).

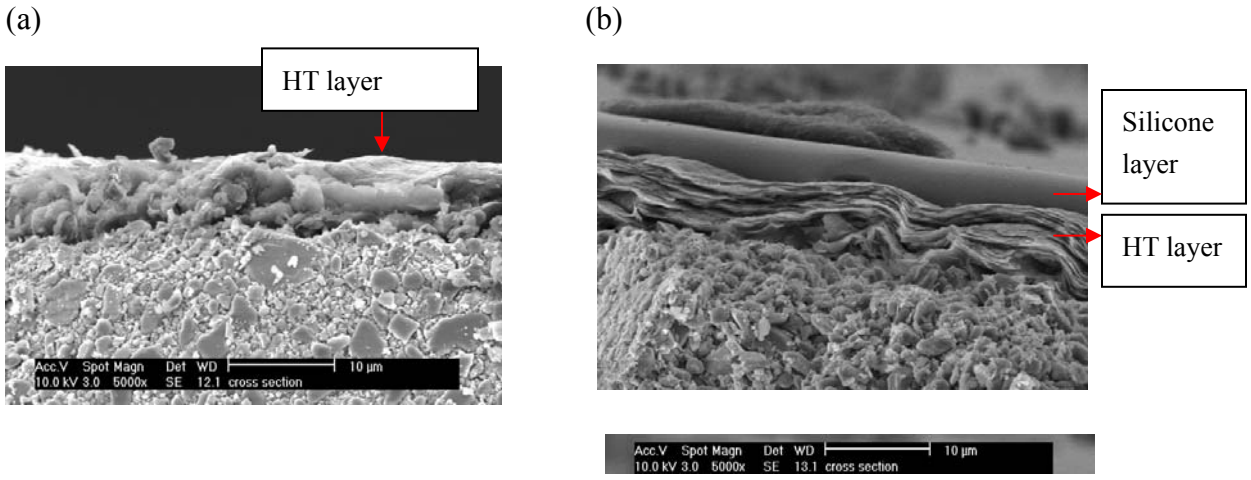


**Figure 9.** The cross-section of (a) a vacuum-suction HT membrane (Magnification ×5K) and (b) silicone-coated vacuum-suction HT membrane (Magnification × 5K).

### 2.2.1.2 Micromembranes

SEM pictures of the microchannel etched on silicon wafers and used for the preparation of micromembranes are presented in Fig. 10.

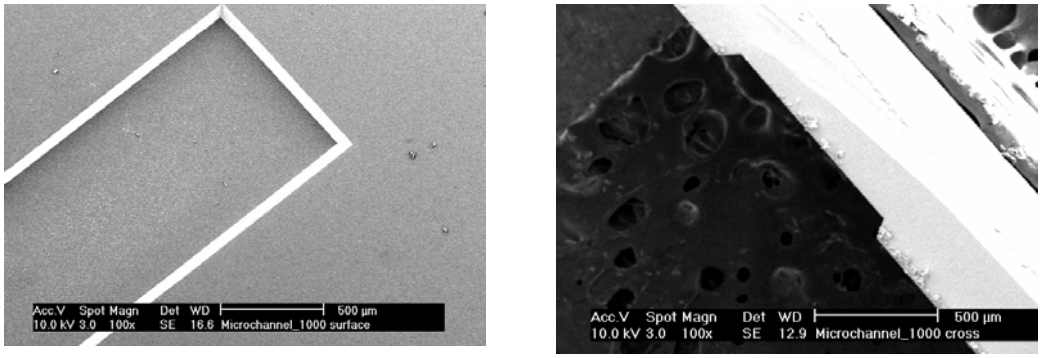


**Figure 10**. SEM picture of Si microchannel (left) top view (right) cross-sectional view

As noted in Table 2, two preparation methods were chosen. SEM observations of the films prepared by seed deposition and hydrothermal aging indicate that they are partially detached layers.

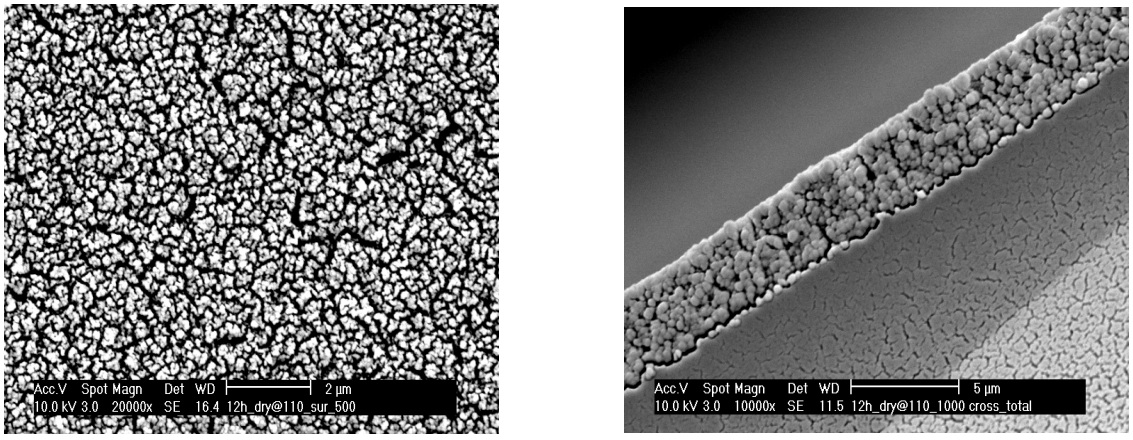


**Figure 11**. SEM pictures of a membrane deposited on a silicon microchannel by coating with a HT colloidal solution. (left) top surface, (right) cross-sectional view

On the other hand, films prepared by direct coating of colloidal HT solutions appear to be well-adhering with a crystallite size in the submicron range. No major defects or

cracks were observed in these films, though some intercrystalline voids exist, as can be seen in the top view and cross-sections of the membrane shown in Fig. 11. To avoid the formation of these voids, a γ-alumina layer was deposited as an intermediate layer on the microchannel prior to HT deposition using a Boehmite sol, and drying the film at 600 $^{o}$C for 2 h.

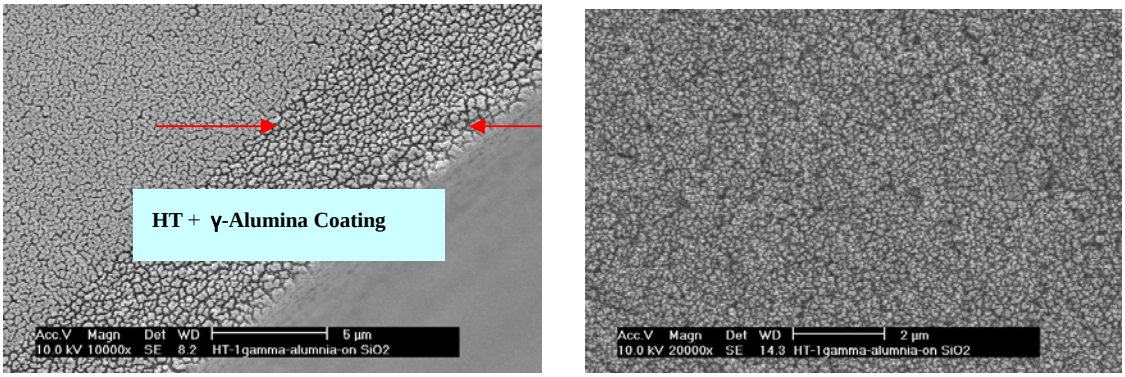


**Figure 12.** HT and alumina layers on the left, and the top HT layer on the right.

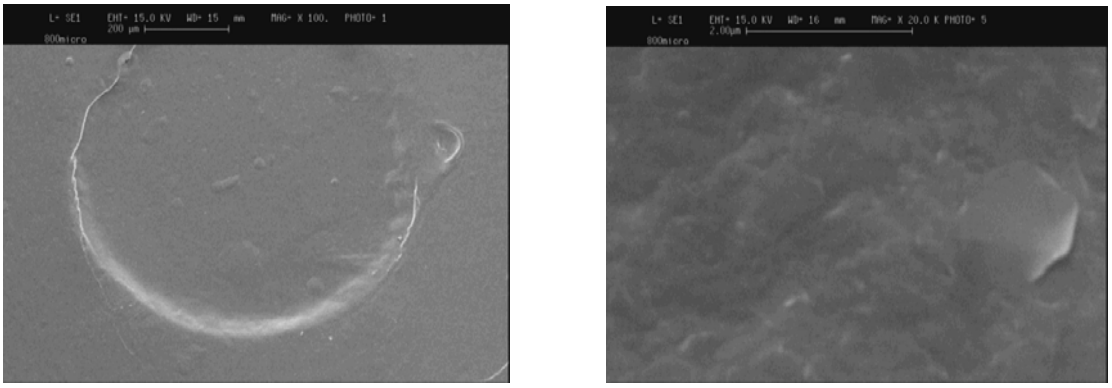

**Figure 13**. SEM picture (top view).of the stainless steel membrane (left) Magnification ×100; (right) Magnification ×20K

Figure 12 shows a cross-sectional view of the γ-alumina intermediate layer and the HT layer deposited on it. The films appear to be well-adhering, the total thickness being ~5 µm, with the thickness of the alumina layer ~1.5 µm. The hydrotalcite crystals in Fig. 12 are similar in appearance to those in Fig. 11, uniform and with dimensions in the

submicron range, albeit much smaller than those in Fig. 11. After the HT coating is prepared on the alumina layer in the microchannel, KOH is used to etch the silicon layer, while leaving the alumina and HT films intact, since alumina has good resistance to the strong base. The resulting HT membranes are then used for permeation tests. These membranes are not very strong mechanically, however, rupturing at pressure gradients larger than 10 psi.

Figure 13 shows the morphology of a membrane prepared on the stainless steel supports (the microhole size in the Figure is ~800 μm). In Fig. 13, the HT membrane surface appears to be smoother than the surface of the membranes on the Si wafers. This is probably because in the preparation of these membranes we have used a different precursor, namely Mg70DS, which has much better dispersion characteristics.

### 2.2.2 Transport Studies

#### 2.2.2.1 Large Area Membranes

*Dip-coating.* The permeation characteristics of membranes (in terms of the ideal separation factor, defined as the ratio of permeances of single gases) prepared using the HT2 hydrotalcite and the procedure described in 2.1.1 are shown in Fig. 14. These membranes were prepared using α-, or γ-alumina tubes. Hydrothermal aging was carried out in an autoclave at various temperatures and times. The permeances measured were typically of the order of $10^{-6}$ [mol/m$^2$ s Pa]. Figure 14 shows the effect of the time of hydrothermal aging (at 80 $^{o}$C) for two different pressure drops. These membranes are slightly permselective towards $CO_2$ (based on Knudsen transport alone, the membrane should favor the permeation of $N_2$, with the $N_2/CO_2$ separation ratio being ~ 1.25). Increasing the temperature of hydrothermal aging slightly improves the permselectivity towards $CO_2$. SEM observation of the top surface of these membranes indicate the presence of visible cracks and defects, however.

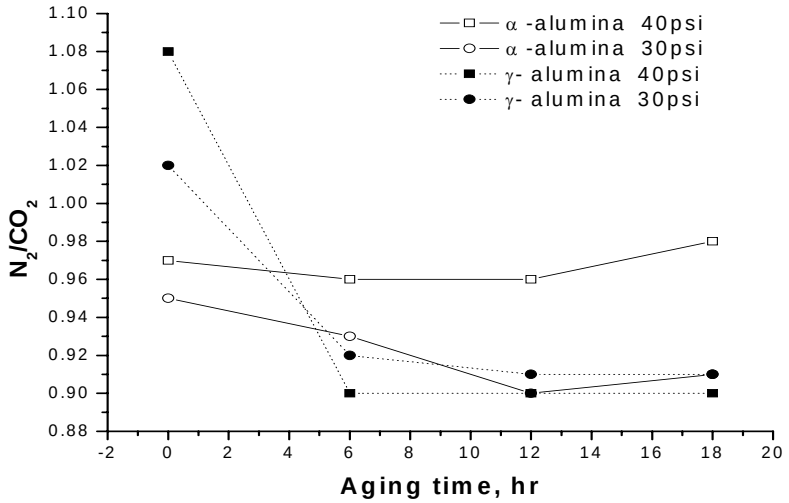


**Figure 14**. The effect of aging time at 80 $^{o}$C on the $N_2/CO_2$ separation factor (Permeation Temp. 25 $^{o}$C).

The permeation characteristics of membranes using the Sasol Mg70D HT according to the procedure described in 5.1.1 are shown in Fig. 15. Two different colloidal dispersions were utilized for dip-coating on α-alumina tubes, one containing 5 wt% of HT (S-5), and the other 1.25 wt% of HT in solution (S-1.25). The effect of the number of coatings utilized to prepare the films is also shown in Fig. 15. Increasing the number of coatings increases the $N_2/CO_2$ separation factor, which levels-off at 1.3 ~ 1.4 (slightly above the Knudsen value ~1.25), which is expected on the basis that increasing the number of coatings, decreases the number of pinholes and cracks, and improves the quality of the resulting membranes. XRD analysis of the membrane surface indicates that is pure hydrotalcite, while SEM indicates a smooth surface with no visible defects and the thickness of the films to be ~5 μm.

*Using Sulfate as a Binder.* As discussed in 2.1.1, a number of membranes were prepared using sulfuric acid as a binder. Table 4 shows the $N_2$ and $CO_2$ permeances and the corresponding $N_2/CO_2$ separation factors (at two different pressure drops of 30 and 40 psi,

and at room temperature) for a number of membranes prepared by this technique. Dip-coating and *in-situ* coating were utilized for membrane preparation from Mg50 and Mg70D HT. The *in-situ* coating method used Mg50 as the HT source, and yielded membranes which were more permselective towards $CO_2$ than the membranes prepared by the dip-coating technique. Membranes prepared by dip-coating were not permselective towards $CO_2$, showing instead a $N_2/CO_2$ separation factor in the range 1.1 - 1.27. The membranes prepared with Mg50 using the sulfate binder were not stable, however, when the temperature was raised above 80 $^oC$.

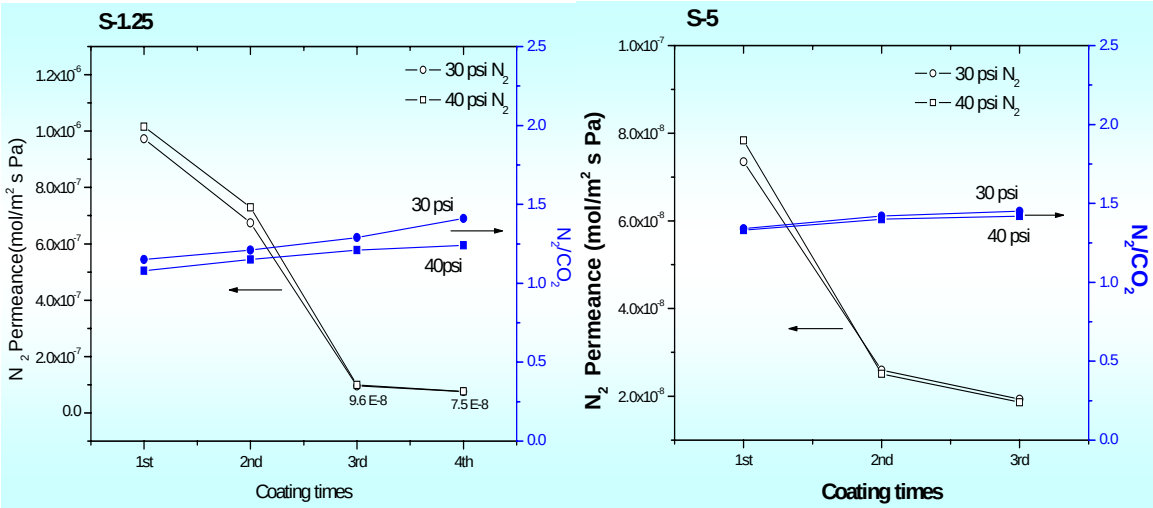


**Figure 15**. The effect of the number of coatings (Permeation Temp. 25 $^oC$).

*Vacuum-Suction Method.* Preparing membranes using vacuum suction may potentially enhance the adhesion of the deposited HT films on the underlying support. A number of membranes using the vacuum-suction method have been prepared, as described in 2.1.1, using the Mg70DS HT, which is prepared by the Mg70D HT powder, by ball-milling at the NETZSCH Corporation.

Table 5 shows the permeance and ideal permselectivity for single gases such as He (a safe surrogate gas for $H_2$), $N_2$ (a safe surrogate gas for CO), Ar and $CO_2$ measured at two different transmembrane pressure drops of 30 or 40 psi and at room temperature, for two

different HT membranes prepared by the vacuum-suction technique. By comparison, the permeance of the underlying alumina support is 2 orders of magnitude higher than that measured with the HT membrane and the separation factors are lower than the Knudsen values, and do not improve significantly as the temperature is raised (from 298 to 503 K), signifying a mostly macroporous structure. The HT membranes are microporous with the most permeable gas being He, followed by $N_2$, Ar, and $CO_2$, with permeances for He in the $10^{-8} \sim 10^{-9}$ mol/m$^2$ s Pa range. Table 6 shows the permeabilities for the HT layer, calculated after one accounts for the permeability of the support layer and the thickness of the HT layer.

**Table 4**. The permeance and the $N_2/CO_2$ separation factor of HT membranes prepared using a sulfate binder (25$^o$C)

| HT source | Coating conditions | Pressure drop (psi) | $CO_2$ | $N_2$ | $N_2/CO_2$ |
|---|---|---|---|---|---|
| Mg50 | Dip-coating, 3 layers | 30 | 2.65E-08 | 3.37E-08 | 1.27 |
| | | 40 | 3.11E-08 | 3.38E-08 | 1.09 |
| | In-situ 30min | 30 | 1.60E-07 | 1.46E-07 | 0.91 |
| | | 40 | 1.82E-07 | 1.65E-07 | 0.90 |
| | In-situ 3 h | 30 | 3.43E-07 | 3.07E-07 | 0.90 |
| | | 40 | 3.96E-07 | 3.56E-07 | 0.90 |
| Mg70D | Dip-coating, 1 layer | 30 | 1.54E-06 | 1.72E-06 | 1.12 |
| | Dip-coating, 3 layers | 30 | 5.63E-07 | 6.93E-07 | 1.23 |

**Table 5**. The permeation characteristics of two HT membranes prepared by the vacuum-suction method (Temp. 25 $^{o}$C)

| Memb | Gas (MW)) | Permeance × $10^{-8}$ (mol/m$^2$ s Pa) | | Permselectivity | | | | | |
|---|---|---|---|---|---|---|---|---|---|
| | | | | He/gas | | | $N_2$/gas | | |
| | | $\Delta P$ | | Ideal Knudsen value | Experimental Result | | Ideal Knudsen value | Experimental Result | |
| | | 30 psi | 40 psi | | 30 psi | 40 psi | | 30 psi | 40 psi |
| su#1 | He (4) | 5.292 | 4.93 | **1.0** | 1.0 | 1.0 | **0.38** | 0.22 | 0.25 |
| | $N_2$ (28) | 1.18 | 1.24 | **2.65** | 4.52 | 3.96 | **1.0** | 1.0 | 1.0 |
| | Ar (40) | 0.873 | 0.883 | **3.16** | 6.08 | 5.60 | **1.20** | 1.35 | 1.42 |
| | $CO_2$ (44) | 0.611 | 0.604 | **3.32** | 8.72 | 8.15 | **1.25** | 1.93 | 2.06 |
| su#23 | He (4) | 2.02 | 1.90 | **1.0** | 1.0 | 1.0 | **0.38** | 0.43 | 0.46 |
| | $N_2$ (28) | 0.869 | 0.881 | **2.65** | 2.32 | 2.16 | **1.0** | 1.0 | 1.0 |
| | $CO_2$ (44) | 0.261 | 0.278 | **3.32** | 7.76 | 6.84 | **1.25** | 3.34 | 3.17 |

**Table 6**.The permeability and ideal selectivity ratio for the HT membrane layers.

| Memb. | $\Delta P$ (psi) | Permeability (Barrer) | | | | Permselectivity | | | |
|---|---|---|---|---|---|---|---|---|---|
| | | He | $N_2$ | Ar | $CO_2$ | $N_2/CO_2$ | $He/CO_2$ | $He/N_2$ | He/Ar |
| su#1 | 30 | 1115.9 | 247.7 | 183.2 | 128.0 | 1.9 | 8.7 | 4.5 | 6.1 |
| Su#23 | 30 | 423.8 | 182.2 | - | 54.6 | 3.3 | 7.8 | 2.3 | - |

[b] Barrer : $10^{-10}$ cm$^3$(STP) ·cm/cm$^2$·s·cmHg =3.35 × $10^{-16}$ mol·m /m$^2$ ·s· Pa

The effect of temperature on permeation for the HT membranes is shown in Table 7. The permeance for all gases decreases as the temperature increases (from 298 to 503 K), with the exception of $CO_2$, which first increases as the temperature increases from 298 to 373, and then subsequently decreases. Table 8 shows the effect of temperature on the HT

layer permeance, showing similar trends.

Notice that the ideal separation factors first decrease with temperature and then increases again. These results can be explained by the surface area and average pore size measurements made with HT powders, shown in Table 3.

**Table 7**. The temperature effect of the HT Su#11 membrane ( $\Delta P$ : 20 psi)

| Temp. | Permeance × $10^{-8}$ (mol/m$^2$ s Pa) | | | | Permselectivity | | | |
|---|---|---|---|---|---|---|---|---|
| (K) | He | $N_2$ | Ar | $CO_2$ | $N_2/CO_2$ | $He/CO_2$ | $He/N_2$ | He/Ar |
| 298 | 2.04 | 0.543 | 0.420 | 0.336 | 1.62 | 6.06 | 3.75 | 4.85 |
| 373 | 1.51 | 0.455 | 0.315 | 0.341 | 1.33 | 4.42 | 3.32 | 4.79 |
| 423 | 1.10 | 0.319 | 0.241 | 0.232 | 1.37 | 4.73 | 3.44 | 4.55 |
| 473 | 0.745 | 0.204 | 0.130 | 0.138 | 1.47 | 5.38 | 3.66 | 5.72 |
| 503 | 0.701 | 0.192 | 0.134 | 0.111 | 1.72 | 6.31 | 3.66 | 5.23 |

**Table 8**. The permeance of the HT layer for the Su#11 membrane. ( $\Delta P$ : 20 psi)

| Temp | Permeance × $10^{-8}$ (mol/m$^2$ s Pa) | | | | Permselectivity | | | |
|---|---|---|---|---|---|---|---|---|
| (K) | He | $N_2$ | Ar | $CO_2$ | $N_2/CO_2$ | $He/CO_2$ | $He/N_2$ | He/Ar |
| 298 | 2.047 | 0.544 | 0.421 | 0.336 | 1.62 | 6.08 | 3.76 | 4.86 |
| 373 | 1.515 | 0.456 | 0.316 | 0.342 | 1.33 | 4.44 | 3.32 | 4.80 |
| 423 | 1.103 | 0.320 | 0.241 | 0.232 | 1.38 | 4.75 | 3.45 | 4.57 |
| 473 | 0.747 | 0.204 | 0.130 | 0.138 | 1.48 | 5.41 | 3.66 | 5.74 |
| 503 | 0.703 | 0.192 | 0.134 | 0.111 | 1.73 | 6.32 | 3.65 | 5.24 |

Note that as the temperature, in which the HT is heat-treated, increases both the mesopore and micropore average pore sizes decrease, consistent with the decrease in the permeance of the various gases.

Table 9 shows the effect of pressure drop on the single gas permeance and the ideal separation factor for three different membrane samples. For He and $N_2$, as the pressure

increases, the permeance first decreases and then increases. For $CO_2$, however, the permeance increases through the whole region of pressures. The ideal separation factor also decreases as a function of pressure. The difference in behavior between He and $N_2$ and $CO_2$ is due to the affinity of the HT structure towards the $CO_2$.

The previous data indicate that the HT membrane is characterized by both microporous and mesoporous regions. However, these membranes appear more selective towards the lower kinetic diameter gases like He, rather than $CO_2$, as one would have expected based on the surface affinity of $CO_2$ in these materials.

**Table 9.** The effect of pressure drop on the permeance and selectivity of the HT membranes (Temp. 25 $^oC$)

| Memb. | $\Delta P$ (psi) | Permeance × $10^{-8}$ (mol/$m^2$ s Pa) | | | Permselectivity | | |
|---|---|---|---|---|---|---|---|
| | | He | $N_2$ | $CO_2$ | $He/CO_2$ | $He/N_2$ | $N_2/CO_2$ |
| Su#22 | 20 | 10.5 | 2.61 | 1.62 | 6.45 | 4.01 | 1.61 |
| | 30 | 9.22 | 2.50 | 1.66 | 5.57 | 3.69 | 1.51 |
| Su#23 | 20 | 2.19 | 0.881 | 0.240 | 9.00 | 2.45 | 3.67 |
| | 30 | 2.02 | 0.869 | 0.261 | 7.74 | 2.32 | 3.33 |
| | 40 | 1.90 | 0.881 | 0.278 | 6.84 | 2.16 | 3.17 |
| Su#25 | 20 | 3.35 | 0.691 | 0.249 | 13.5 | 4.85 | 2.78 |
| | 30 | 3.15 | 0.659 | 0.331 | 9.5 | 4.79 | 1.99 |
| | 40 | 3.27 | 0.688 | 0.394 | 8.3 | 4.75 | 1.75 |

In order to probe the intrinsic properties of the HT materials, we used a silicone material, as previously described, composed of vinyl-polydimethylsiloxane (VPDMS) and modified silica to coat the membrane. This silicone compound has good thermal resistance, with operational temperature as high as 204 $^oC$. To study the effect of coating the membrane with the silicone layer, we first measured the properties of the membrane

without the coating, and then after the membrane was coated we measured its transport properties again. After silicone coating, the HT membrane permeance significantly decreases, as shown in Table 10. The same Table shows the permeances and separation factors of silicone membrane coated on an alumina disk. Assuming a resistance in series model for the silicone on alumina membrane itself, we have calculated the permeability and ideal separation factors for the silicone layer (based on its thickness measured from the SEM pictures). The values are shown in Table 11, where they are compared with corresponding values of PDMS from the literature. Using this permeability value and the measured thickness of the silicone layer on the HT membrane, we calculate the permeances and ideal selectivities of the HT membrane itself (HT layer + alumina support). The calculated and experimental values are compared in Table 12.

**Table 10.** Permeation properties before and after silicone-coating. Permeance units: $\times 10^{-9}$ (mol/m$^2$ s Pa), 25 $^o$C

| $\Delta P$ (psi) | Gas | Before coating | | After coating | | Silicone-coated alumina membrane | |
|---|---|---|---|---|---|---|---|
| | | Permeance | $CO_2/N_2$ | Permeance | $CO_2/N_2$ | Permeance | $CO_2/N_2$ |
| 30 | $N_2$ | 26.5 | 0.68 | 0.0159±0.0014 | 31.1± 2.5 | 0.204 | 9.6 |
| | $CO_2$ | 18.1 | | 0.494±0.002 | | 1.97 | |
| 40 | $N_2$ | 24.9 | 0.70 | 0.0165±0.0013 | 27.3± 1.8 | 0.204 | 10.0 |
| | $CO_2$ | 17.5 | | 0.450±0.008 | | 2.04 | |

The experimental values are significantly higher than the calculated ones, which signifies that the silicone layer penetrates into the underlying support structure. It is likely that the calculated ideal separation factors reflect the affinity of the $CO_2$ molecules for the intercrystalline space of the hydrotalcite material itself. Table 13 shows the permeation characteristics of a different membrane, including the permeances of smaller molecules

like He and $H_2$. Again the silicone-coated membranes show enhanced $CO_2$ permeation. The reported ideal separation factors of the silicone-coated membrane significantly exceed those of the silicone membrane itself, pointing out that the separation characteristics of the silicone-coated HT membrane reflect the intrinsic properties of the HT material.

**Table 11**. The permeabilities and ideal selectivities of the silicone coating (Temp. 25 °C)

| $\Delta P$ (psi) | Permeability (Barrer) | | | | Ideal S.F. for $CO_2/N_2$ | | Refs. |
|---|---|---|---|---|---|---|---|
| | Experiment | | Reference (PDMS) | | Experiment | Reference | |
| | $CO_2$ | $N_2$ | $CO_2$ | $N_2$ | | | |
| 15 | | | 2645 | 251.9 | | 10.5 | 15 |
| 30 | 19.44 | 2.01 | 1300 | 299 | 9.61 | 4.35 | 16 |
| 40 | 20.13 | 2.01 | - | - | 9.95 | - | |

**Table 12**. The comparison between calculated and experimental values for the HT membrane (Temp. 25 °C)

| $\Delta P$ (psi) | Permeance $\times 10^{-9}$ (mol/m$^2$ s Pa) | | | | Permselectivity $CO_2/N_2$ | |
|---|---|---|---|---|---|---|
| | Calculated | | Experimental | | Calc. | Exp. |
| | $CO_2$ | $N_2$ | $CO_2$ | $N_2$ | | |
| 30 | 0.659 | 0.0172 | 18.1 | 26.5 | 38.23 | 0.68 |
| 40 | 0.577 | 0.0180 | 17.5 | 24.9 | 32.15 | 0.70 |

*Electrophoretic Deposition*. Table 14 shows the permeance and permselectivity of a number of EPD membranes prepared under various preparation conditions. Most HT-EPD membranes exhibit Knudsen flow, with the exception of membranes E6, E7, and E8. E6 was also used for mixed gas mixture permeation tests (see discussion below). The morphology of these membranes has been studied by SEM. Using Mg70DS results is

smooth HT layers, while, on the other hand, the surface of the membranes prepared by the synthetic HT appears rougher. For most of the membranes in Table 14 the thickness was ~ 15 μm.

**Table 13.** The permeation characteristics of a silicone-HT membrane and silicone membrane

| Memb. | $\Delta P$ (psi) | Permeance × $10^{-9}$ (mol/m$^2$·sec·Pa]) | | | | Permselectivity | | |
|---|---|---|---|---|---|---|---|---|
| | | $CO_2$ | $N_2$ | He | $H_2$ | $CO_2/N_2$ | $CO_2/H_2$ | $CO_2$/He |
| Silicone HT | 30 | 0.546± 0.003 | 0.0159± 0.0014 | 0.0440± 0.0005 | 0.108± 0.001 | 34.4±3.1 | 5.0±0.1 | 12.4±0.1 |
| | 40 | 0.489± 0.009 | 0.0165± 0.0013 | 0.0504± 0.0016 | 0.102± 0.001 | 29.7±1.8 | 4.8±0.1 | 9.70±0.2 |
| Silicone | 30 | 1.97 | 0.204 | 0.291 | 0.504 | 9.6 | 3.9 | 6.8 |
| | 40 | 2.04 | 0.204 | 0.296 | 0.516 | 10.0 | 3.9 | 6.9 |

### 2.2.2.2 Micromembranes

Single gas permeation tests (for He, Ar, $CO_2$, $N_2$, at ΔP=30 psi, and at room temperature) were also conducted with the micromembranes prepared on the stainless steel supports. Figure 16 shows the measured permeances and the ideal permselectivities for various gas pairs. The order of permeance was He>$CO_2$>Ar, according to their kinetic diameters. For $N_2$, however, the permeance is smaller than that of $CO_2$ but larger than that of Ar. Based on the measured He/Ar permselectivity, the membrane is microporous. The measured permeances for the micromembranes are smaller than those of the other

**Table 14.** The permeance and permselectivity of EPD membranes

| Name | Support | EPD conditions | | | | $N_2$ Permeance ($mol/m^2sPa$) | | $N_2/CO_2$ | |
|---|---|---|---|---|---|---|---|---|---|
| | | voltage /coating times | Time | pH | Solution | ΔP | | ΔP | |
| | | | | | | 30 psi | 40 psi | 30 psi | 40 psi |
| E1 | α-$Al_2O_3$ Tube | 1V/1 | 24 h | 12 | Synth. HT | $1.5\times10^{-7}$ | $1.6\times10^{-7}$ | 1.16 | 1.05 |
| E2 | γ-$Al_2O_3$ Tube | 2V/4 | 24h | 12 | Synth. HT | $2.7\times10^{-7}$ | $2.9\times10^{-7}$ | 1.13 | 1.17 |
| E3 | α-$Al_2O_3$ disc | 2V/3 | 24h | 12 | Synth. HT | $2.6\times10^{-7}$ | $3.0\times10^{-7}$ | 1.13 | 1.03 |
| E4 | S-5[a] | 1V/1 | 1 h | 7 | Mg70DS[b] | $2.1\times10^{-7}$ | - | 1.28 | - |
| E5 | HT disc | 1V/1 | 3h | 7 | Mg70DS | $6.6\times10^{-7}$ | $7.0\times10^{-7}$ | 1.33 | 1.29 |
| E6 | α-$Al_2O_3$ Tube | 1V/1 | 1.5h | 7 | Mg70DS | $5.4\times10^{-7}$ | - | 0.83 | - |
| E7 | S-5[c] | 20V/3 | 1h | 7 | Mg70DS | $2.7\times10^{-7}$ | $3.8\times10^{-7}$ | 0.75 | 0.88 |
| E8 | S-5[c] | 20V/2 | 1h | 7 | Mg70DS | $2.0\times10^{-7}$ | - | 0.86 | - |

Temperature of Permeation: 25 $^oC$: [a] HT dip coating on the inside by S-5(5wt% Mg70D); [b]: 0.76wt% Mg70DS;[c]: HT dip coating on outside by S-5(5wt% Mg70D)

membrane discussed, so far, potentially due to the larger thickness of these membranes (the permeance for $CO_2$ was $2\times10^{-9}$ [$mol/m^2$ s Pa], as an example, which is 4 times smaller than that of the vacuum suction HT membranes, for which the average permeance

was $8.8\times10^{-9}$ [mol/m$^2$ s Pa]).

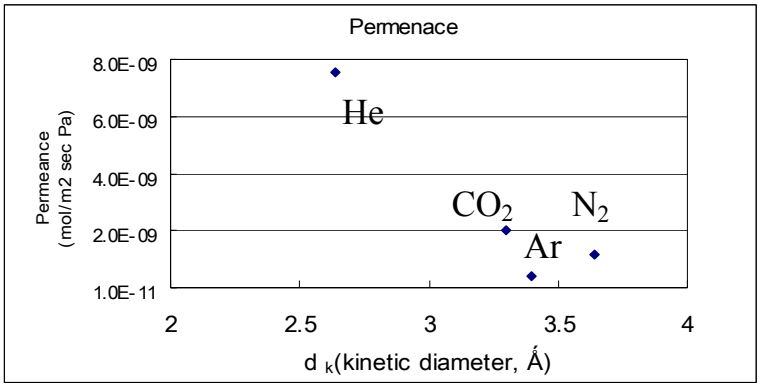


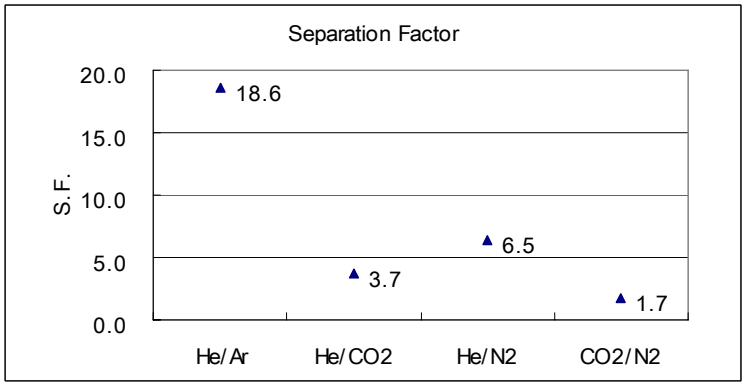


**Figure 16**. The permeance (a) and permselectivity (b) of micromembrane prepared on stainless steel supports.

### 2.2.2.3. Transport Studies with Gas Mixtures

Several membranes were also tested for the permeation of gas mixtures. Table 15 shows the results for the $N_2/CO_2$ gas pair ($N_2$ is used here as a safe surrogate gas for CO). The mixed gas separation factor for the various membranes were generally very similar to the separation factor based on single gas permeances. Table 16 shows effect of temperature on the permeance and separation factor of the $CO_2/N_2$ gas mixture using the E6 membrane. The $CO_2$ permeance and the separation factor for membrane E6 increase as temperature increases. On the other hand, the $N_2$ permeance decreases as temperature

increases.

**Table 15**. The comparison between single gas and gas mixture separation factors

| Membrane | Number of Coatings | Separation Factor($N_2/CO_2$) | |
|---|---|---|---|
| | | Single gas | Gas Mixture |
| Dipcoating [a] by 1.25 wt% Mg70D solution | 4 | 1.3 | 1.4 |
| Dipcoating [a] by 5wt% Mg70D solution | 2 | 1.27 | 1.4 |
| EPD E#6 [b] | EPD 1 coating | 0.83 | 0.72 |

P= 30psi; R.T. ; Feed gas composition: $N_2$:$CO_2$=0.4:0.6,

[a]: α-alumina tube, [b]: Feed gas $N_2$:$CO_2$=0.7:0.3

**Table 16**. The temperature effect of the E6 membrane for mixture of gases

| Temp.(K) | Permeance $\times 10^{-7}$ (mol/m$^2$sPa) | | Separation Factor ($CO_2/N_2$) |
|---|---|---|---|
| | $CO_2$ | $N_2$ | |
| 298 K | 4.38 | 3.15 | 1.39 |
| 423 K | 4.69 | 2.86 | 1.64 |
| 473 K | 5.05 | 2.49 | 2.03 |

△P= 30psi, Feed gas $N_2$:$CO_2$=0.7:0.3

## 2.3 Conclusions

We have presented here results of our studies, whose goal is the preparation of affinity-type $CO_2$-selective membranes. In the preparation of these membranes, we have

used a number of hydrotalcite (HT) sources, prepared in our laboratories and also available commercially; we have also used a variety of mesoporous and macroporous supports, including HT porous disks prepared in our laboratories, and alumina tubes and disks. We have also prepared two types of membranes, large area membrane disks and tubes, and micromembranes prepared on stainless steel foils and silicon wafers. The micromembranes show good potential for application in micro-fuel cells. The membranes have been tested for their transport characteristics using both single gases and mixtures of gases, as well as by a variety of other characterization techniques including SEM and TEM, DRIFTS, EDX, and DTA/TGA. Quality nanoporous membranes have been prepared which show significantly higher permeation rates for gases with smaller kinetic diameters like He (used here as a safe surrogate gas for hydrogen) as compared to gases with larger kinetic diameters like Ar. Some of these membranes are selective towards $CO_2$. The effect of preparation conditions on the membrane transport characteristics have also been studied and are reported here. Coating these membranes with a silicone layer improves their separation characteristics making them significantly more permeable towards $CO_2$, as one would have expected based on the strong affinity of these materials towards $CO_2$.

**3. Milestones**

All important milestones set for this project have been accomplished.

**4. Cost and Schedule Status**

Initial Project Budget: $ 50,000

Costs Incurred During the Project: $ 50,000.00

Funds Remaining: $ 0.

## 5. Summary of Significant Accomplishments

The following are some of the key accomplishments:

- We have developed and studied a number of techniques for the preparation of HT membranes.
- Different membranes have been developed, characterized and tested for their permeation characteristics towards single gases and mixtures of gases.
- A number of these membranes were shown to be nanoporous, and some of them show good permselectivity towards $CO_2$.

## 6. Actual or Anticipated Problems or Delays

The project was on schedule and no delays occurred.

## 7. Technology Transfer Activities Accomplished

A paper is in preparation, and will be submitted to Industrial Engineering Chemistry Research. Results of this research were presented at the 2006 AIChE Annual Meeting in San Francisco.

## 8. References


1. Roelofs, C. A. A.; Bokhoven, J. A.; Dillen, A. J.; Geus, J. W.; Jong, K. P., "The thermal decomposition of Mg-Al hydrotalcites: Effects of interlayer anions and characteristics of the final structure", *Chem. Eur. J.*, 2002, 8, N0.24.
2. Gardner, E.; Huntoon, K. M.; Pinnavaia, T. J., "Direct synthesis of alkoxide intercalate derivatives of hydrotalcite-like layered double hydroxides: Precursors for the formation of colloidal layered double hydroxide suspensions and transparent thin films", *Adv. Mater*., 2001, 13, 1263.
3. Arai, T., "Proton conductive membrane and production method thereof", *U. S. Patent Application Publication*, 2004, US20040081823A1.
4. Huang, A.; Lin, Y. S.; Yang, W., "Synthesis and properties of A-type zeolite membranes by secondary growth method with vacuum seeding", *Journal of Membrane Science*, 245, 2004, 41-51.
5. Cortez, G.., "Separation, real-time migration monitoring and selective zone retrieval using a computer controlled system for automated analysis", *Appl. Theor. Electrophoresis*, 1995, 4, 197-209.
6. Delgado, A. V., "Interfacial electrokinetics and electrophoresis", Marcel Deker, Inc., 2002.
7. Seike, T.; Matsuda M.; Miyake, M., "Fabrication of Y-type zeolite films by electrophoretic deposition" *Solid State Ionics*, 151, 2002, 123– 127.
8. Datta, S., "Application of design of experiment on electrophoretic deposition of glass-ceramic coating materials from an aqueous bath", *Bull. Mater. Sci*., Vol. 23, No. 2, April 2000, 125–129.
9. "Electrophoresis – Electrophoretic Deposition as Coating Technique", www. AZoM.com
10. Chen, C. Y.; Chen, S. Y.; Liu, D. M., "Electrophoretic deposition forming of porous alumina membranes", *Acta Mate*r., Vol. 47, No. 9, 1999, 2717-2726.

11. Oonkhanond, B.; Mullins, M. E., "The preparation and analysis of zeolite ZSM-5 membrane on porous alumina supports", *Journal of Membrane Science*, 194, 2001, 3-13.
12. Madou, M. J., "Fundamentals of microfabrication" 2nd, CRC Press, 2002.
13. Wan, Y. S. S.; Chau, J. L. H,; Gavriilidis, A.; Yeung, K. L., "Design and fabrication of zeolite-based microreactors and membrane microseparators", *Microporous and Mesoporous Materials*, 32, 2001, 157-175
14. Reichle, W.T., "Synthesis of anionic clay minerals (mixed metal hydroxides, Hydrotalcite)", *Solid State Ionics*, 22, 1986, 135.
15. Pravven Jha, Larry W. Mason, J. Douglas Way, Journal of Membrane Science 272, 125-136, 2006.
16. Christopher J. Orme, Mark L. Stone, Michael T. Benson, and Eric S. Peterson Separation Science and Technology 38 (12, 13), 3225–3238, 2003.